nature materials

LETTERS

PUBLISHED ONLINE: 7 JULY 2013 | DOI: 10.1038/NMAT3698

Core–shell strain structure of zeolite microcrystals

Wonsuk Cha[1], Nak Cheon Jeong[2†], Sanghoon Song[3], Hyun-jun Park[1], Tung Cao Thanh Pham[2], Ross Harder[4], Bobae Lim[5], Gang Xiong[6], Docheon Ahn[7], Ian McNulty[8], Jungho Kim[5], Kyung Byung Yoon[2,3], Ian K. Robinson[6,9] and Hyunjung Kim[1,3*]

Zeolites are crystalline aluminosilicate minerals featuring a network of 0.3–1.5-nm-wide pores, used in industry as catalysts for hydrocarbon interconversion, ion exchangers, molecular sieves and adsorbents[1]. For improved applications, it is highly useful to study the distribution of internal local strains because they sensitively affect the rates of adsorption and diffusion of guest molecules within zeolites[2,3]. Here, we report the observation of an unusual triangular deformation field distribution in ZSM-5 zeolites by coherent X-ray diffraction imaging[4], showing the presence of a strain within the crystal arising from the heterogeneous core–shell structure, which is supported by finite element model calculation and confirmed by fluorescence measurement. The shell is composed of H-ZSM-5 with intrinsic negative thermal expansion[5] whereas the core exhibits a different thermal expansion behaviour due to the presence of organic template residues, which usually remain when the starting materials are insufficiently calcined. Engineering such strain effects could have a major impact on the design of future catalysts.

Zeolites, having subnanometre-scale pores lined with chemically active surfaces, are widely used as catalysts, sorbents, ion exchangers, molecular separation membranes[6–14], membrane reactors[15] and many others[1]. Although each zeolite has well-defined pore sizes and shapes, they could undergo a significant degree of distortion if the zeolite crystal is situated under a strongly strained condition. If this happens the rates of adsorption of molecules into the zeolite channels, subsequent diffusion within the channels, and desorption from the channels to the exteriors will be greatly altered. Although structural changes of crystals have often been measured by X-ray and neutron powder diffraction[16,17], these diffraction techniques are sensitive only to the ensemble average of many crystals, and do not resolve local structural variations within individual crystals, such as the differences between their cores and outermost parts. Elucidation of the three-dimensional patterns, degrees, and causes of internal strains will greatly help to explain the observed chemical activity and adsorption behaviour of zeolites, and to design appropriate conditions to tune and enhance this behaviour for applications.

ZSM-5 is an aluminosilicate zeolite having 5.5 Å × 5.1 Å elliptical channels running along the *a* axis in a sinusoidal manner and 5.6 Å × 5.3 Å elliptical channels running straight along the *b* axis. This zeolite is usually synthesized from gels containing a Si source, an Al source, tetrapropylammonium hydroxide (TPAOH), a base and water. The use of TPAOH is necessary because the TPA^+ ions act as the structure-directing agents. As a result, these organic ions become entrapped at the intersections between the sinusoidal and straight channels, thereby blocking the channels[18]. Therefore, they must be removed from ZSM-5 crystals by calcination[19] (usually by heating at 450–550 °C for several hours under flowing oxygen or air) before the crystals can be used for catalysis, adsorption and separation. However, if the zeolite is calcined at lower temperatures or calcined not long enough even at the required temperatures, corks or residual carbon compounds can remain in the crystals, thereby still partially blocking the channels.

ZSM-5 crystals have complex temperature-dependent anisotropic thermal expansion coefficients[5,17,20,21]. Accordingly, each crystal undergoes anisotropic thermal expansion during the initial stage and anisotropic thermal contraction during the later stage of calcination, that is, in the 25–150 °C and 150–550 °C regions, respectively.

Here, we report on an unusual internal deformation field distribution in a micrometre-sized crystal of ZSM-5 by coherent X-ray diffraction imaging[4] (CDI). We used ZSM-5 crystals supported on a silicon substrate as a model system to study the formation of strain under various calcination conditions.

When a crystal is illuminated by a coherent X-ray beam and the crystal dimensions are smaller than the coherence volume of the beam, the scattering from all parts of the sample can interfere to form a coherent X-ray diffraction (CXD) pattern. The phase of the scattered wave can be reconstructed from the CXD pattern intensity by numerical phase retrieval to form an image of the sample. Internal deformations of the sample crystal lattice are evident in the reconstructed complex amplitude as phase shifts. These arise from the asymmetric part of the diffraction pattern at each Bragg reflection; the symmetric part can be considered to come from the internal electron density of the crystal[4,22,23].

A schematic of the CDI experiment geometry in which the (200) reflection of a ZSM-5 microcrystal was measured in nitrogen is shown in Fig. 1a. Typically, CXD patterns are expected to show characteristic Airy ring patterns around the Bragg peak at the centre and a vertical streak attributed to its (200) facets[22] (see Supplementary Fig. S1). From the diffraction patterns as a function of temperature with different calcination conditions, we have observed a range of patterns between the two extremes shown in Fig. 1b,c. Figure 1b shows a diffraction pattern indicating a relatively unstrained state of the crystal, whereas Fig. 1c exhibits a more distorted diffraction pattern: the shape at the centre of Bragg peak is triangular and the fringes are no longer along the crystal axes. The perpendicular section of the three-dimensional

[1]Department of Physics, Sogang University, Seoul 121-742, Korea, [2]Department of Chemistry, Sogang University, Seoul 121-742, Korea, [3]Interdisciplinary Program of Integrated Biotechnology, Sogang University, Seoul 121-742, Korea, [4]Advanced Photon Source, Argonne National Laboratory, Argonne, Illinois 60439, USA, [5]Department of Life Sciences, Sogang University, Seoul 121-742, Korea, [6]London Centre for Nanotechnology, University College, London WC1H 0AH, UK, [7]Pohang Accelerator Laboratory, Pohang 790-784, Korea, [8]Center for Nanoscale Materials, Argonne National Laboratory, Argonne, Illinois 60439, USA, [9]Research Complex at Harwell, Didcot, Oxford OX11 0DE, UK. †Present address: Department of Emerging Materials Science, Daegu Gyeongbuk Institute of Science & Technology (DGIST), Daegu 711–873, Korea. *e-mail: hkim@sogang.ac.kr

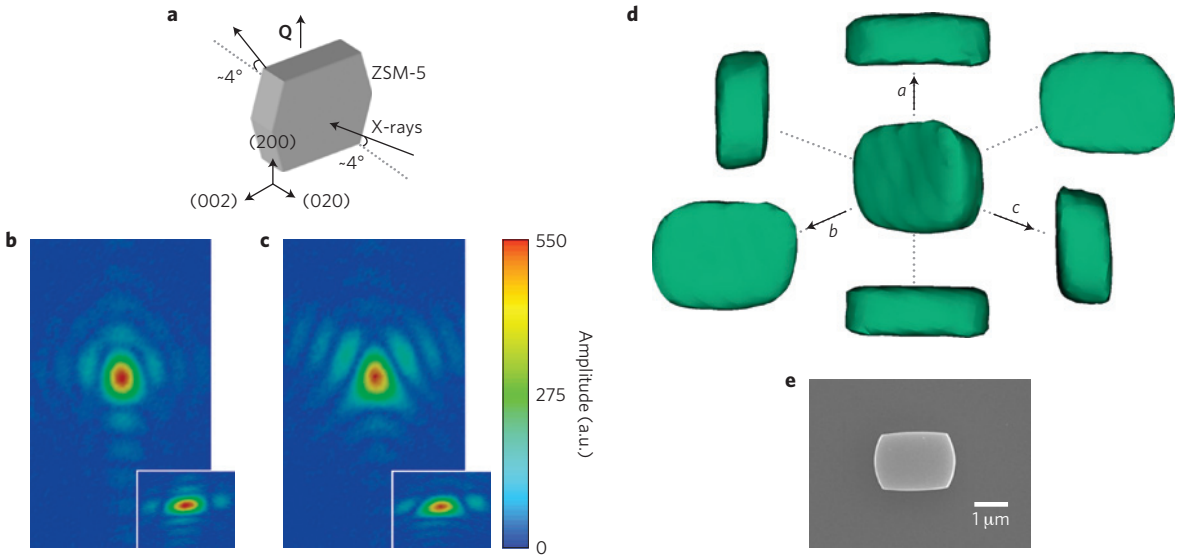

Figure 1 | CXD patterns and three-dimensional image of a ZSM-5 zeolite crystal. a, The geometry of a ZSM-5 zeolite microcrystal attached to a silicon wafer in the CDI experiment. The momentum transfer wavevector **Q** for (200) Bragg reflection, determined by the direction of incident and scattered X-rays, is shown. **b**, Diffraction pattern of a ZSM-5 crystal before heating measured by a CCD detector in the geometry shown in **a**. **c**, The same crystal after heating to 200 °C. The insets in **b**,**c** show perpendicular views of the three-dimensional patterns. **d**, Three-dimensional real-space image of the ZSM-5 microcrystal reconstructed from three-dimensional CXD patterns by the phase retrieval algorithm. The projected images parallel to the *a*, *b* and *c* axes are shown. **e**, A typical SEM image of the sample along the *b* axis.

diffraction patterns at 90° (in the bottom-right panels in Fig. 1b,c for each case) do not show such distorted shape, implying that the distortions are mostly confined to the (020) plane of the crystal.

A phase retrieval algorithm was applied to the data to phase the measured diffraction patterns. We used error reduction and hybrid input–output methods[24] with the restricted phase (because the phases are not changed beyond that range) and with finite supports as the real-space constraints. Once phased, the three-dimensional data were inverted to real space by Fourier transformation and a coordinate transformation. Further details are given in the Supplementary Information. In Fig. 1d, a 37.5% isosurface of the resulting density of the three-dimensional image of a ZSM-5 crystal (Si/Al ~ 130) in the triangular strained state is shown, and its shape is shown from several directions. The entire shape shows a close resemblance to the scanning electron microscope (SEM) image of a crystal with a more common (020) orientation from the same batch, shown in Fig. 1e.

The development of internal crystal strains, invisible to SEM, is the main focus of the present work. The inversion of the data to a complex density function also yields a real-space phase value for every point in space, which we illustrate as a colour scale ranging from blue (−1 rad) to red (+1 rad). The phase is interpreted quantitatively as a projection onto the momentum transfer **Q**-vector of the local displacement of the crystal from an ideal undistorted lattice[4]. A phase of $\pi/2$ corresponds to a shift (along **Q**) of one-quarter of (200) lattice spacing, or 0.25 nm. Figure 2 shows the phase maps of the crystals from the same batches intersecting through its centre as a function of temperature with different calcination conditions. The positive phase (red) indicates displacement along **Q** whereas the negative phase (blue) that in the opposite direction. In the crystals calcined at 450 °C for 3 h and 12 h, initially unstrained, they begin to strain at 100 °C and reach a maximum at 200 °C. The maximum strain component is seen with a total phase excursion of 1.8 radians, corresponding to a total displacement of about 29% of ZSM-5 (200) spacing, that is, 0.29 nm. This means that the spatial derivative of displacement along the entire size (~2.0 μm) of the crystal is $\sim 10^{-4}$. In the image at 200 °C, the edges of the sample are compressed but the centre part is expanded along **Q**‖[200]. The deformation becomes smaller and more uniform with further increasing temperature. However, the crystals calcined at 550 °C (independent of time) do not show strong displacement evolution. Note that the development of the triangular strained state on heating was observed in almost all of the crystals independent of crystal size, aluminium concentration and the existence of copper atoms. Only the calcining temperature was found to affect this behaviour.

Even though calcining at 450 °C might leave a residue of the TPA inside the crystals, it is not clear how residual organic templates can give rise to the unusual and transient appearance of strained material inside the crystal. Therefore, we first measured the existence of the organic template residue by element analysis. The results in Supplementary Table S1 show that ZSM-5 crystals calcined at 550 °C do not contain any residual TPA whereas those calcined at 450 °C (independent of the calcination time) have minute amounts of nitrogen and carbon compounds. To find out where those residual organics are located, energy dispersive X-ray (EDX) spectroscopy and confocal fluorescence microscopy[25] were employed. In EDX measurements, the crystals calcined at 550 °C and 450 °C for 3 h were found to contain residual organic template material. The relative atomic compositions measured at several positions of an individual crystal in Supplementary Fig. S2(a) calcined at 550 °C and Supplementary Fig. S2(b) calcined at 450 °C are shown in Supplementary Tables S2 and S3, respectively. Among the composition of the organic templates, nitrogen was below the detection limit, but the carbon concentration was higher in the crystal calcined at 450 °C. In that sample, the centre part shows a slightly higher concentration of carbon. As the level of the absolute amount of carbon is very low, the distribution fluctuated from sample to sample.

On the basis of the observation above, fluorescence from organic templates (not completely decomposed) within ZSM-5 was measured by confocal fluorescence microscopy[25]. The fluorescence from the crystal calcined at 450 °C is shown in Supplementary Fig. S3(a) (also in Fig. 4d) in the range of 420–515 nm excited with a 405 nm laser. Owing to the very low concentration combined with the size of the crystal being close to the resolution limit, the fluorescence signal was very weak. The image obtained with the sum of 10 measurements shows an inhomogeneous density

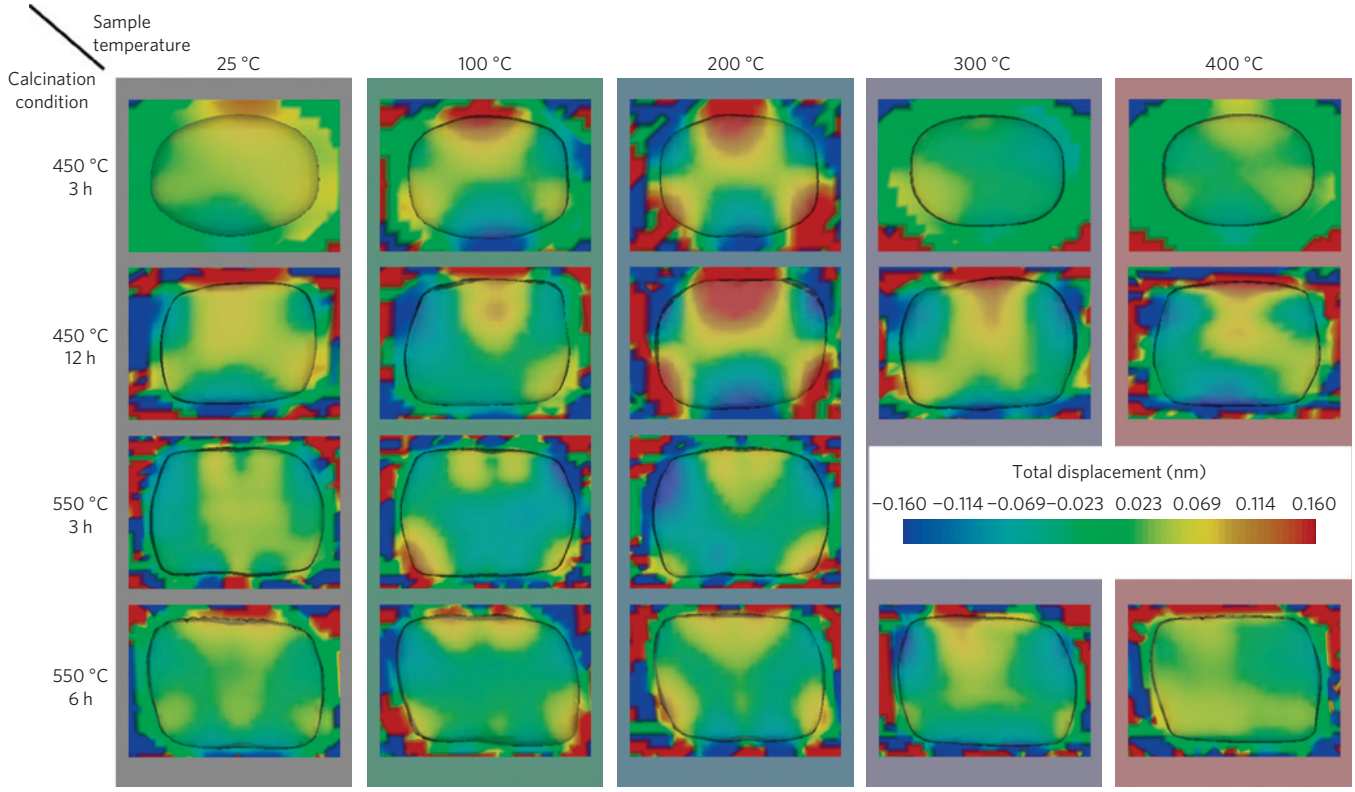

Figure 2 | Internal phase images depending on calcination condition as a function of temperature. Lattice displacement is shown as a map of phase, intersecting through the centre part of the crystals down their *b* axis. The phase interpreted as the scalar product of the local deformation and the momentum transfer wavevector **Q** shows a marked change in the sample calcined at 450 °C. The triangular pattern appears at 200 °C and disappears with increasing temperature. However, this observation is not seen in the sample calcined at 550 °C. The colour scale represents a range of ±1 radian corresponding to the displacement of ±0.160 nm. A positive value (red) means that the lattice moved in the same direction as **Q** whereas a negative value (blue) means that it moved in the opposite direction.

of organic materials; that is, the centre part is higher than the outer part. From the sample calcined at 550 °C, however, no fluorescence was detected.

To determine the effect of organic templates on the thermal expansion behaviour of ZSM-5, we applied high-resolution X-ray powder diffraction (HRPD) to as-synthesized ZSM-5 to compare the thermal expansion of calcined ZSM-5 (550 °C for 12 h and 450 °C for 3 h; curve A and B in Fig. 3, respectively) with as-synthesized material (before calcining; curve C). The HRPD data are shown in Supplementary Fig. S4. The variation of the lattice parameters of ZSM-5 along the *a*, *b*, *c* axes, and the unit-cell volume, are shown in Fig. 3a–d (in vacuum), and Fig. 3e–h (in nitrogen atmosphere), respectively. Differences in lattice parameter (Δd) are calculated with respect to the value of A at 25 °C for each condition. The overall behaviours of A and B are very similar, but C showed slope changes in thermal expansion. Along the *a* axis, curve A exhibits negative thermal expansion whereas curve C exhibits positive thermal expansion up to 300 °C (in vacuum) and 250 °C (in nitrogen) and negative thermal expansion thereafter. The lattice changes from curve B show a similar behaviour to the negative thermal expansion observed in A, but slightly positive thermal expansion is observed up to 150 °C. Along the *b* and *c* axes, thermal expansion behaviours for curve C do not show notable differences up to ∼350 °C in vacuum, whereas the slope changes from positive to negative at 250 °C in nitrogen. Note that in nitrogen the values from curves A and C approach the same values at 400 °C. This explains why triangular strain is released at 400 °C, shown in Fig. 2.

All of the information above allows us to model the strain pattern and resulting X-ray diffraction patterns using finite element analysis (FEA). The process is described in detail in the Supplementary Information. We assume an inhomogeneous distribution of residual organic TPA template material within the crystal allowing the shape and area of distribution of residues, that is, without giving any spatial constraints. The imaged phase $\varphi(\mathbf{r}) = \mathbf{Q} \cdot \mathbf{u}(\mathbf{r})$, where $\mathbf{u}(\mathbf{r})$ is the local displacement of the crystal from an ideal undistorted lattice at position $\mathbf{r}$ inside the sample, is sensitive to the *a* axis displacement only at the (200) reflection used, which is the direction with opposite sign in thermal expansion of ZSM-5 before and after calcination. The centre region, containing TPA, expands on heating, whereas the border regions contract.

The FEA results in Fig. 4a–c simulated for 200 °C use effective thermal expansion coefficients derived from Fig. 3: $\alpha_a = -3.790 \times 10^{-6}\,\mathrm{K}^{-1}$, $\alpha_b = 3.392 \times 10^{-6}\,\mathrm{K}^{-1}$ and $\alpha_c = -7.945 \times 10^{-7}\,\mathrm{K}^{-1}$ for the three principal axis directions of the sample after calcination at 550 °C in nitrogen, and $\alpha_a = 7.246^{-6}\,\mathrm{K}^{-1}$, $\alpha_b = 2.572 \times 10^{-6}\,\mathrm{K}^{-1}$ and $\alpha_c = 3.390 \times 10^{-6}\,\mathrm{K}^{-1}$ for those before calcination. The detailed thermal expansion coefficients are shown in Supplementary Table S4. We modelled the crystal with its actual dimensions rigidly bonded to a silicon substrate. Further information can be obtained in the Supplementary Information. The simulation we found that worked was based on inhomogeneities of the expansion coefficients, best illustrated by the core–shell structure in Fig. 4a. The spatial distribution of organic templates shows a complete agreement with that obtained from the fluorescence mapping. It also agrees with the fact that the core has a positive coefficient whereas the shell has negative expansion. From the calculation with the intrinsic negative thermal expansion of ZSM-5 and positive thermal expansion of silicon, shown in Fig. 4b, a gradual change in displacement is obtained along the crystal with no evidence of triangular deformation. Differential thermal expansion

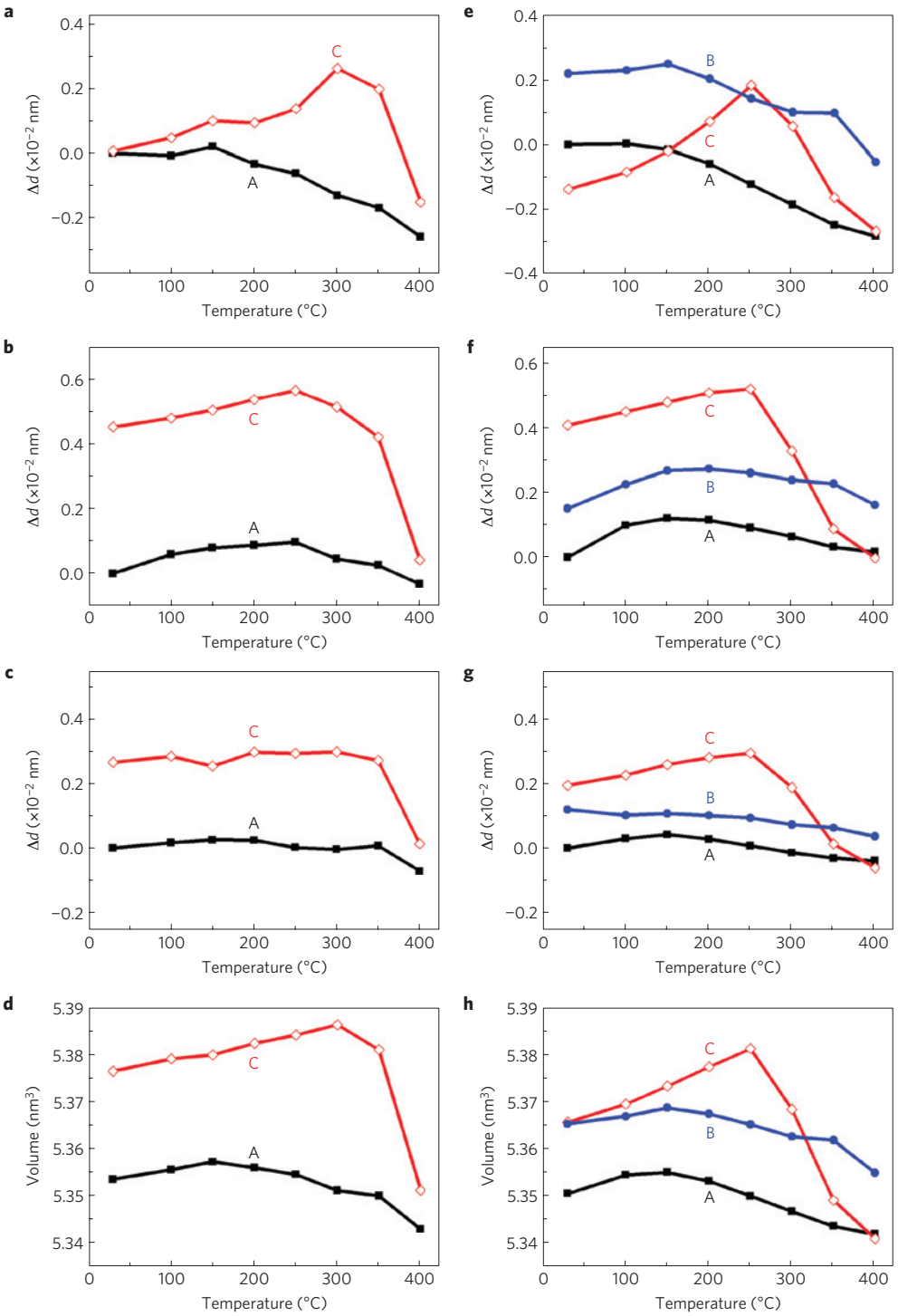

Figure 3 | Measured thermal expansion behaviour of ZSM-5 calcined at 550 °C (A), 450 °C (B), and as-synthesized before calcination (C). a–h, The change of lattice parameters of ZSM-5 along the *a*, *b* and *c* axes and the volume of the unit cell of ZSM-5 measured by HRPD experiments in vacuum (**a–d**) and in nitrogen atmosphere (**e–h**). The lattice difference (Δd) is calculated by subtracting the value of A at 25 °C from the measured value at each temperature.

effects alone were unable to explain the observed structure. Owing to the positive expansion of the substrate, calculations with another combination of thermal expansion coefficients shown in Fig. 4c did not obtain the observed displacement pattern. Figure 4d is the same image shown in Supplementary Fig. S3(a) expanded by 1.6 times for comparison.

Other possible scenarios for explaining the unique triangular shape of strain patterns could be an inhomogeneous distribution of aluminium[26]. Evidence of variations of aluminium concentration between the rim and the centre of the crystals has been found in our samples by X-ray microfluorescence experiments (see Supplementary Fig. S5). This, together with the variation of the lattice parameter with aluminium content observed in ZSM-5 (ref. 21), might give the core–shell structure and hence a similar strain pattern. However, it should not be dependent on the calcination conditions because changes in the 200–300 °C range are

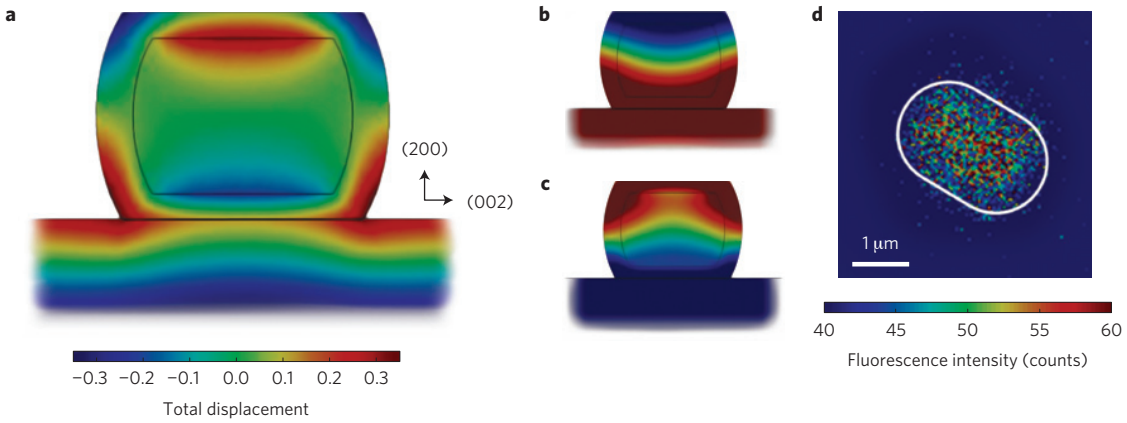

Figure 4 | FEA simulation of displacement distribution at 200 °C with core–shell structure and confocal fluorescence microscope image. a, The best model that produces the triangular displacement distribution. The calculation was set to have the positive thermal expansion coefficient of the core and negative thermal expansion coefficient of the shell. The magnitude of vertical displacement shown agrees with that measured by CDI in Fig. 2. The colour scale bar indicates the amount of total displacement on a nanometre scale. Positive values shown in red mean that the point moves up, whereas negative values mean that the point moves down. **b**, The result due to the known intrinsic negative thermal expansion behaviour of ZSM-5 attached to a silicon substrate exhibits a gradual pattern, which does not agree with our experimental result. **c**, The same as model **a**, with exchanged thermal expansion coefficients of the core and the shell; the resultant pattern does not agree with observation. **d**, Localized residual templates detected with a confocal fluorescence microscope. Fluorescence in the range of 420–515 nm excited with a laser with 405 nm of wavelength shows an inhomogeneous distribution that allows modelling with FEA. The white solid line indicates the edge of the crystal and the rainbow-coloured scale bar shows the fluorescence intensity. Details are in the Supplementary Information.

unlikely to be due to redistribution of aluminium atoms within the crystal. However, the strain could easily be explained by the organic template material, as in our model.

In this study, we have observed an internal deformation distribution in ZSM-5 zeolite microcrystals bonded to silicon substrates. The fully calcined crystals remain relaxed with a relatively small displacement field within the crystal, as resolved along the (200) **Q**-vector in our CDI method. Although the distribution of residual organic impurities can be detected by other techniques, the strain field distribution inside the crystal due to such small traces was detectable only by CDI. Before they are fully calcined, the crystals adopt a transient triangular strained state, maximally developed at 200 °C, with a characteristic pattern of displacements, which can be attributed to a core–shell arrangement of strain with an inhomogeneous distribution of lattice parameters. The best model includes also the effects of differential expansion with respect to the substrate. This deformation propagates through the crystal to create a reversed pattern of displacements on the opposite side. The appearance of strain also depended on the starting state and temperature history in a way that is consistent with trapping of the organic TPA template material in the inner volume of the crystal. The macroscopic deformation seen in these small crystals affects adsorption and diffusion of molecules through the pores.

Methods

Sample preparation. ZSM-5 crystals were synthesized by hydrothermal reaction from gels consisting of tetraethyl orthosilicate (TEOS), sodium aluminate ($NaAlO_2$; 35% Na_2O, and 35% Al_2O_3), TPAOH and KOH. To obtain crystals with different Si/Al ratios, the gels were composed of $TEOS/NaAlO_2/TPAOH/H_2O = 7.0:0.28:1.0:600.0$ for Si/Al ~ 130 and $TEOS/NaAlO_2/TPAOH/KOH/H_2O = 8.0:0.4:1.0:0.4:500.0$ for Si/Al ~ 60 or ~90. The gels were reacted at 180 °C for 5 h and 200 °C for 24 h in an autoclave for Si/Al~130 and Si/Al~60 to 90, respectively. The produced ZSM-5 crystals were isolated using centrifugation and subsequently washed with distilled deionized water several times. A colloidal solution, in which ZSM-5 crystals were dispersed in a dilute solution of polyethylene imine dissolved in ethanol, was used for crystals to be isolated onto a silicon substrate. Subsequently, the samples were calcined at either 450 °C or 550 °C for several hours in air. During the calcination, Si–O–Si chemical bonds were formed between the surface of zeolite and the Si substrate from terminal Si–OH groups by dehydration.

CDI experiments. Unfocused coherent X-rays with a wavelength of 0.1380 nm from the 34-ID-C beamline in the Advanced Photon Source illuminated isolated samples mounted in a sample chamber in nitrogen environment with varying temperature. CXD patterns were measured with a CCD (charge-coupled device) detector with 22.5 μm^2 pixels located about 2 m away from the sample. Three-dimensional diffraction data were collected as rocking curves of the sample tilt angle with steps of 0.01° or 0.016° with a total of 31 to 51 frames.

Confocal fluorescence microscopy. Fluorescence measurements were carried out with a confocal microscope (a Leica TCS SPE with a Leica DMI4000 B upright microscope) with 4 laser lines (405, 488, 532 and 635 nm). Emission spectra were measured in the range of 420–515, 505–555, 545–655 and 645–735 nm for 4 laser lines, respectively. Samples (ZSM-5 with dimensions of $1.88 \times 0.78 \times 2.68\ \mu m^3$ and silicalite-1 with $3.0 \times 1.0 \times 9.5\ \mu m^3$ along the *a*, *b* and *c* axes of the crystals, respectively) were placed on a cover glass and calcined before the measurements.

Thermal expansion of ZSM-5. The HRPD experiments in vacuum and in nitrogen atmosphere were performed at the 9B beamline in the Pohang Light Source, Korea. The $20 \times 1\ mm^2$-sized X-rays with a wavelength of 0.15494 nm or 0.15475 nm illuminated ZSM-5 as a function of temperature. The data were collected with a multi-detector system of seven detectors with analysers located with an installation angle of 20°. Owing to the high crystalline structure of ZSM-5, the diffraction was measured with a step size of 0.005°.

FEA. The COMSOL MULTIPHYSICS package was used for FEA of the displacement along the different thermal expansion behaviours in a ZSM-5 crystal. The ZSM-5 was modelled to have a core–shell structure with different thermal expansion coefficients measured by high-resolution X-ray diffraction. To simplify the simulation, the rectangular parallelepiped with curved sides was used with the same dimensions measured by SEM, that is, $1.88 \times 0.78 \times 2.68\ \mu m^3$ along the *a*, *b* and *c* axes of ZSM-5, respectively.

Received 20 January 2012; accepted 23 May 2013; published online 7 July 2013

References

1. Davis, M. E. Ordered porous materials for emerging applications. *Nature* **417,** 813–821 (2002).
2. Smit, B. & Maesen, T. L. M. Towards a molecular understanding of shape selectivity. *Nature* **451,** 671–678 (2008).
3. Kärger, J. Single-file diffusion in zeolites. *Mol. Sieves Sci. Technol.* **7,** 329–366 (2008).
4. Robinson, I. & Harder, R. Coherent X-ray diffraction imaging of strain at the nanoscale. *Nature Mater.* **8,** 291–298 (2009).
5. Park, S. H., Kunstleve, R-W. G., Graetsch, H. & Gies, H. The thermal expansion of the zeolites MFI, AFI, DOH, DDR, and MTN in their calcined and as synthesized forms. *Stud. Surf. Sci. Catal.* **105,** 1989–1994 (1997).

6. Lai, Z. *et al.* Microstructural optimization of a zeolite membrane for organic vapor separation. *Science* **300,** 456–460 (2003).
7. Choi, J. *et al.* Grain boundary defect elimination in a zeolite membrane by rapid thermal processing. *Science* **325,** 590–593 (2009).
8. Pham, T. C. T., Kim, H. S. & Yoon, K. B. Growth of uniformly oriented silica MFI and BEA zeolite films on substrates. *Science* **334,** 1533–1538 (2011).
9. Lee, J. S., Lee, Y.-J., Tae, E. L., Park, Y. S. & Yoon, K. B. Synthesis of zeolite as ordered multicrystal arrays. *Science* **301,** 818–821 (2003).
10. Caro, J. & Noack, M. in *Advances in Nanoporous Materials,* Vol. 1 (ed. Ernst, S.) Ch. 1, 1–96 (Elsevier, 2009).
11. Caro, J. & Noack, M. Zeolite membranes—Recent developments and progress. *Micropor. Mesopor. Mater.* **115,** 215–233 (2008).
12. O'Brien-Abraham, J. & Lin, J. Y. S. in *Zeolites in Industrial Separation and Catalysis* (ed. Kulprathipanja, S.) Ch. 10, 307–329 (Wiley, 2010).
13. O'Brien-Abraham, J., Kanezashi, M. & Lin, Y. S. Effects of adsorption-induced microstructural changes on separation on xylene isomers through MFI-type zeolite membranes. *J. Membr. Sci.* **320,** 505–513 (2008).
14. Hedlund, J., Jareman, F., Bons, A-J. & Anthonis, M. A masking technique for high quality MFI membranes. *J. Membr. Sci.* **222,** 163–179 (2003).
15. Bein, T. Synthesis and applications of molecular sieve layers and membranes. *Chem. Mater.* **8,** 1636–1653 (1996).
16. Jeong, H. -K., Lai, Z., Tsapatsis, M. & Hanson, J. C. Strain of MFI crystals in membranes: An *in situ* synchrotron X-ray study. *Micropor. Mesopor. Mater.* **84,** 332–337 (2005).
17. Marinkovic, B. A. *et al.* Complex thermal expansion properties of Al-containing HZSM-5 zeolite: A X-ray diffraction, neutron diffraction and thermogravimetry study. *Micropor. Mesopor. Mater.* **111,** 110–116 (2008).
18. Chao, K-J., Lin, J-C., Wang, Y. & Lee, G. H. Single crystal structure refinement of TPA ZSM-5 zeolite. *Zeolites* **6,** 35–38 (1986).
19. Gao, X., Yeh, C. Y. & Angevine, P. Mechanistic study of organic template removal from ZSM-5 precursors. *Micropor. Mesopor. Mater.* **70,** 27–35 (2004).
20. Gualtieri, M. L., Gualtieri, A. F. & Hedlund, J. The influence of heating rate on template removal in silicalite-1: An *in situ* HT-XRPD study. *Micropor. Mesopor. Mater.* **89,** 1–8 (2006).
21. Sen, S., Wusirika, R. R. & Youngman, R. E. High temperature thermal expansion behavior of H[Al]ZSM-5 zeolites: The role of Brønsted sites. *Micropor. Mesopor. Mater.* **87,** 217–223 (2006).
22. Pfeifer, M. A., Williams, G. J., Vartanyants, I. A., Harder, R. & Robinson, I. K. Three-dimensional mapping of a deformation field inside a nanocrystal. *Nature* **442,** 63–66 (2006).
23. Newton, M. C., Leake, S. J., Harder, R. & Robinson, I. K. Three-dimensional imaging of strain in a single ZnO nanorod. *Nature Mater.* **9,** 120–124 (2010).
24. Fienup, J. R. Phase retrieval algorithms: a comparison. *Appl. Opt.* **21,** 2758–2769 (1982).
25. Karwacki, L. & Weckhuysen, B. M. New insight in the template decomposition process of large zeolite ZSM-5 crystals: An *in situ* UV-Vis/fluorescence micro-spectroscopy study. *Phys. Chem. Chem. Phys.* **13,** 3681–3685 (2011).
26. Ballmoos, R. & Meier, W. M. Zoned aluminium distribution in synthetic zeolite ZSM-5. *Nature* **289,** 782–783 (1981).

Acknowledgements

This research was supported by the Basic Science Research Program through the National Research Foundation of Korea (NRF) funded by the Ministry of Education and the Ministry of Science, ICT & Future Planning of Korea (Nos. 2007-0053982, 2011-0012251 and 2008-0062606, CELA-NCRC), Sogang University Research Grant of 2012 and an ERC FP7 Advanced Grant 227711. W.C. was also supported by a Hi Seoul Science/Humanities Fellowship from the Seoul Scholarship Foundation. K.B.Y. thanks the NRF project No. 2012M1A2A2671784. G.X. and I.K.R. were supported by the 'Nanoscupture' advanced grant from the European Research Council. Use of the Advanced Photon Source was supported by the US Department of Energy, Office of Science, Office of Basic Energy Science, under Contract No. DE-AC02-06CH11357.

Author contributions

H.K. supervised and coordinated all aspects of the project. ZSM-5 growth was carried out by N.C.J. and T.C.T.P. under the supervision of K.B.Y. Coherent X-ray diffraction measurements were carried out by W.C., S.S., H-j.P., R.H., I.K.R. and H. K. CDI data analysis was carried out by W.C. and R.H. Energy-dispersive X-ray spectra measurements were performed by T.C.T.P. and W.C. Confocal fluorescence microscopy measurements were carried out by B.L. and W.C. under the supervision of J.K. and H.K. Powder diffraction measurements were carried out by W.C., S.S., H-j.P. and D.A. and data analysis done by W.C. H-j.P. and D.A. Finite element analysis calculation was carried out by G.X., R.H. and W.C. under the supervision of I.K.R and H.K. W.C., R.H. and I.M. carried out X-ray microfluorescence measurements. W.C., K.B.Y., I.K.R. and H.K. wrote the paper. All authors discussed the results and commented on the manuscript.

Additional information

Supplementary information is available in the online version of the paper. Reprints and permissions information is available online at www.nature.com/reprints. Correspondence and requests for materials should be addressed to H.K.

Competing financial interests

The authors declare no competing financial interests.